Constraints on Climate Sensitivity from Radiation Patterns in Climate Models

MARKUS HUBER, IRINA MAHLSTEIN, AND MARTIN WILD

Institute for Atmospheric and Climate Science, Zürich, Switzerland

JOHN FASULLO

National Center for Atmospheric Research, Boulder, Colorado

RETO KNUTTI

Institute for Atmospheric and Climate Science, Zürich, Switzerland

(Manuscript received 31 August 2009, in final form 24 August 2010)

ABSTRACT

The estimated range of climate sensitivity, the equilibrium warming resulting from a doubling of the atmospheric carbon dioxide concentration, has not decreased substantially in past decades. New statistical methods for estimating the climate sensitivity have been proposed and provide a better quantification of relative probabilities of climate sensitivity within the almost canonical range of 2–4.5 K; however, large uncertainties remain, in particular for the upper bound. Simple indices of spatial radiation patterns are used here to establish a relationship between an observable radiative quantity and the equilibrium climate sensitivity. The indices are computed for the Coupled Model Intercomparison Project phase 3 (CMIP3) multimodel dataset and offer a possibility to constrain climate sensitivity by considering radiation patterns in the climate system. High correlations between the indices and climate sensitivity are found, for example, in the cloud radiative forcing of the incoming longwave surface radiation and in the clear-sky component of the incoming surface shortwave flux, the net shortwave surface budget, and the atmospheric shortwave attenuation variable β. The climate sensitivity was estimated from the mean of the indices during the years 1990–99 for the CMIP3 models. The surface radiative flux dataset from the Clouds and the Earth's Radiant Energy System (CERES) together with its top-of-atmosphere Energy Balanced and Filled equivalent (CERES EBAF) are used as a reference observational dataset, resulting in a best estimate for climate sensitivity of 3.3 K with a likely range of 2.7–4.0 K. A comparison with other satellite and reanalysis datasets show similar likely ranges and best estimates of 1.7–3.8 (3.3 K) [Earth Radiation Budget Experiment (ERBE)], 2.9–3.7 (3.3 K) [International Satellite Cloud Climatology Project radiative surface flux data (ISCCP-FD)], 2.8–4.1 (3.5 K) [NASA's Modern Era Retrospective-Analysis for Research and Application (MERRA)], 3.0–4.2 (3.6 K) [Japanese 25-yr Reanalysis (JRA-25)], 2.7–3.9 (3.4 K) [European Centre for Medium-Range Weather Forecasts Re-Analysis (ERA-Interim)], 3.0–4.0 (3.5 K) [ERA-40], and 3.1–4.7 (3.6 K) for the NCEP reanalysis. For each individual reference dataset, the results suggest that values for the sensitivity below 1.7 K are not likely to be consistent with observed radiation patterns given the structure of current climate models. For the aggregation of the reference datasets, the climate sensitivity is not likely to be below 2.9 K within the framework of this study, whereas values exceeding 4.5 K cannot be excluded from this analysis. While these ranges cannot be interpreted properly in terms of probability, they are consistent with other estimates of climate sensitivity and reaffirm that the current climatology provides a strong constraint on the lower bound of climate sensitivity even in a set of structurally different models.

1. Introduction

The earth's climate system is almost entirely driven by shortwave radiative energy coming from the sun. Although temperature and precipitation are the most widely recognized climate variables, it is basically the radiation with its energy flows and balances within the climate system that determines the earth's climate and thus drives its various internal processes and feedbacks. Changes in the concentration of atmospheric constituents result in a perturbation of the earth's radiation balance; hence, the adequate representation of the radiative fluxes in the climate system is a prerequisite for any climate model. Local-to-global-scale observations of the radiative fluxes include surface (SFC) radiation

Corresponding author address: Markus Huber, Institute for Atmospheric and Climate Science, Universitätstrasse 16, CHN N 16.1, ETH Zürich, CH-8092 Zurich, Switzerland.
E-mail: markus.huber@env.ethz.ch

DOI: 10.1175/2010JCLI3403.1

measurements, for example, the Baseline Surface Radiation Network (BSRN; Ohmura et al. 1998) and the Global Energy Balance Archive (GEBA; Ohmura and Gilgen 1991) as well as satellite-derived data products such as ERBE (refer to Table 2 for expansion of dataset names; Ramanathan et al. 1989) and the CERES experiment (Wielicki et al. 1996). The advent of improved observational datasets and comprehensive radiative transfer models recently allowed the production of the first 18-yr global gridded radiative flux profile dataset stemming from the ISCCP-FD encompassing both full- and clear-sky fluxes at five levels in the atmosphere, starting from the surface up to the top-of-atmosphere (TOA) (Zhang et al. 2004). Reanalyses are a powerful tool to combine satellite measurements and data output from numerical models and provide a comprehensive representation of the radiative fluxes in climate system. Among the most recent reanalyses are the National Aeronautics and Space Administration (NASA)'s MERRA project (available online at http://gmao.gsfc.nasa.gov/research/merra/), the ECMWF Re-Analysis (ERA-Interim, available online at http://www.ecmwf.int/research/era/do/get/era-interim), and JRA-25 (Onogi et al. 2007). In terms of modeling the radiative fluxes, a review of the developments in radiation budget modeling in general circulation models (GCMs) from a surface perspective over the last few decades, up to the latest generation of GCMs used in the Fourth Assessment Report (AR4) of the Intergovernmental Panel on Climate Change (IPCC) can be found in Wild (2008). A long-standing problem of AOGCMs is that they overestimate the shortwave and underestimate the longwave downward radiation at the surface (Wild 2008).

Simple indices of surface air temperature patterns, such as the global-mean, the land–ocean contrast, the annual cycle (AC), and the interhemispheric difference (NS), were used in previous studies to describe global climate variability and change (Karoly and Braganza 2001; Braganza et al. 2003, 2004). The observed temperature, radiation fields, and trends have been extensively used to constrain climate sensitivity and future temperature projections (Forest et al. 2002; Harvey and Kaufmann 2002; Knutti et al. 2002; Gregory et al. 2004; Murphy et al. 2004; Knutti et al. 2006, 2008; Sanderson et al. 2008a). Here we use and extend the indices defined in Braganza et al. (2003) and look at surface and TOA radiation patterns during the period lasting from 1990 to 1999 for the multimodel dataset of the World Climate Research Programme Coupled Model Intercomparison Project phase 3 (WCRP CMIP3) and correlate them with the corresponding climate sensitivities of the different climate models. An estimate of climate sensitivity is inferred by comparing the linear relationship described above to observational reference data for the corresponding period. To relate some of the radiative indices to physical feedbacks, we compute the same indices for the total cloud cover, the column-integrated atmospheric water vapor content, and the sea ice concentration.

Despite an unprecedented effort in climate modeling and an increase in computing power and observational data, the uncertainty in predicting the response of the climate system to a doubling of atmospheric carbon dioxide levels, defined as equilibrium climate sensitivity, has not substantially decreased (Meehl et al. 2007). The AR4 estimated a likely range for climate sensitivity of 2–4.5 K, similar to the range of 1.5–4.5 K estimated in the Third Assessment Report (TAR), but with a slight increase of the lower bound. Probability distribution functions indicate nonzero probabilities for climate sensitivities outside that range (Knutti and Hegerl 2008). While the spread of climate sensitivity derived from various multimodel ensembles mostly resulted in the range between 2 and 4.5 K, the multi-thousand-member ensemble from Climateprediction.net (CPDN) sampled a broader range from 2 to more than 11 K (Stainforth et al. 2005). Several studies employing the CPDN perturbed physics ensemble find a best estimate of climate sensitivity of around 3.3 and between 3 and 3.5 K (Piani et al. 2005; Knutti et al. 2006). Despite the broad range of possible climate sensitivities suggested by the CPDN models, the best estimates still lie in the range of 2–4.5 K encompassed by the multimodel ensembles. The long-standing, main uncertainty for both equilibrium and transient runs stems from the representation of cloud feedbacks, with the spread in cloud feedbacks as computed by various GCMs being roughly 3 times larger than the one accounting for the combined water vapor–lapse-rate feedback, the radiative forcing, or the ocean heat uptake (Cess et al. 1989; Dufresne and Bony 2008). A review of the concept of the equilibrium climate sensitivity and the methods to estimate its range can be found in Knutti and Hegerl (2008) and Allen et al. (2006).

Our goal is to account for model biases in the estimation of climate sensitivity by establishing statistically significant regressions between simulated sensitivities and model biases, and then applying observed constraints to these regressions. The focus of our efforts will be on regions and fluxes that are key in explaining the spread of GCM radiative feedbacks under climate change.

This paper is structured as follows. Section 2 outlines the model and observational data employed in this study. It also introduces the radiative indices and the notion of constraining unmeasurable quantities in the climate system, such as the equilibrium climate sensitivity by using an intermodel correlation obtained from

the radiative indices and the climate sensitivities computed by the CMIP3 multimodel dataset. These indices, the intermodel correlations to climate sensitivity, and the kernel density estimates for the latter are shown in section 3, where also some illustrative examples are depicted. Section 4 discusses some issues of uncertainty involved in our method. A summary and conclusions are presented in section 5.

2. Data and methods

a. Model data

This study employs AOGCM model output for the twentieth-century integrations obtained from the CMIP3 data archive (available online at http://www-pcmdi.llnl.gov/ipcc/about_ipcc.php). All available all-sky (as) and clear-sky (cs) radiation fields were taken into account. Because of the inconsistency of aerosol forcing agents across the CMIP3 models, as shown in Table 10.1 of Meehl et al. (2007), we did not use any aerosol data. In addition to the radiation fields, we used the monthly averaged fields of the total cloud cover (variable clt), the atmospheric water vapor (prw), and sea ice concentration (sic). To have a homogeneous set of grids and consistency with the zonal definition of the indices, the available monthly averaged fields were interpolated to a T42 grid. The models and their corresponding climate sensitivities are listed in Table 1.

TABLE 1. The climate models and their corresponding equilibrium climate sensitivities used in this study. Model identifications (IDs) and climate sensitivity values are taken from Table 8.2 of Randall et al. (2007). Further information on the models can be found in Table 8.1. of Randall et al. (2007).

Model ID	Equilibrium climate sensitivity (°C)
CCSM3	2.7
CGCM3.1(T47)	3.4
CSIRO-MK3.0	3.1
CGCM3.1(T63)	3.4
ECHAM5/MPI-OM	3.4
ECHO-G	3.2
FGOALS-g1.0	2.3
GFDL-CM2.0	2.9
GFDL-CM2.0	3.4
INM-CM3.0	2.1
IPSL-CM4	4.4
MIROC3.2(hires)	4.3
MIROC3.2(medres)	4.0
MRI-CGCM2.3.2	3.2
PCM	2.1
UKMO-HadCM3	3.3
UKMO-HadGEM1	4.4

b. Observational and reanalysis datasets

As an observational dataset, we employ the 5-yr climatological radiation fields for the surface and TOA fluxes derived from CERES (Wielicki et al. 1996). Raw CERES data from the *Terra* FM1 instrument were used for the surface fluxes and the EBAF fields (CERES EBAF) for the TOA fluxes. For the CERES surface data, clear-sky incoming and outgoing fluxes were not available, only the clear-sky net shortwave and longwave budgets. We use a modified CERES dataset that matches the TOA imbalance by Hansen et al. (2005) (refer to section 4). As a satellite reference dataset for the TOA, we also use the data from the ERBE during the years 1985–1989. Because of the failure of the National Oceanic and Atmospheric Administration's *NOAA-9* satellite, we employ here the ocean-to-land energy-transport-adjusted ERBE product of Fasullo and Trenberth (2008), which incorporates also an adjustment to the outgoing longwave TOA radiation. The comprehensive radiative surface and TOA flux dataset from the ISCCP-FD (Zhang et al. 2004) is also taken into account. The ISCCP-FD dataset is the successor of the previous ISCCP-FC project and incorporates both an improved NASA Goddard Institute for Space Studies (GISS) radiative transfer model as well as more advanced satellite-retrieval algorithms. Moreover, the observations specifying the input for the radiative transfer model have also improved. Because of the surface and TOA biases in the ISCCP-FD dataset (Zhang et al. 2004) and errors in the angular distribution models of ERBE, the use of CERES data is deemed superior.

In terms of reanalysis data, the satellite data products of CERES, ERBE, and ISCCP-FD are complemented by NASA's Global Modeling and Assimilation Office (GMAO) MERRA covering the years 1979 to present (available online at http://gmao.gsfc.nasa.gov/research/merra/intro.php) and JRA-25, which was developed at the Japan Meteorological Agency (JMA) and Central Research Institute of Electric Power Industry (CRIEPI). Six-hourly forecast radiation datasets were available for the period 1979–2009 (Onogi et al. 2007). We also use data from the ERA-40 project, which is a 45-yr reanalysis of the global atmosphere and surface conditions from September 1957 to August 2002, carried out by the ECMWF in Reading, United Kingdom (Uppala et al. 2005), and the NCEP–NCAR reanalysis starting in 1948 (Kalnay et al. 1996). Further, the ERA-Interim dataset is taken into account, which is the successor of the ERA-15 and ERA-40 reanalyses. ERA-Interim covers the period 1989 to present (available online at http://www.ecmwf.int/research/era/do/get/era-interim). This new reanalysis dataset has more extensive features than the previous datasets; that is, it includes additional cloud parameters and more pressure levels. Both the ERA-40

TABLE 2. Observational reference datasets and their corresponding periods used in this study. See text for further details and references.

Dataset	Period
Clouds and the Earth's Radiant Energy System (CERES) (surface) and Energy Balanced and Filled Equivalent (EBAF) (TOA)	2000–05
Earth Radiation Budget Experiment (ERBE)	1985–88
The International Satellite Cloud Climatology Project radiative surface flux data (ISCCP-FD)	1984–99
NASA's Modern Era Retrospective-Analysis for Research and Applications (MERRA)	1979–99
Japanese 25-yr Reanalysis (JRA-25)	1979–99
European Centre for Medium-Range Weather Forecasts (ECMWF) ERA-Interim Reanalysis (ERA-I)	1989–99
The 40-yr ECMWF Re-Analysis (ERA-40)	1958–99
The National Centers for Environmental Prediction–National Center for Atmospheric Research (NCAR; NCEP) reanalysis project	1948–99

and ERA-Interim datasets do not contain solar clear-sky downward and upward surface fluxes. The online distribution of ERA-40 data does not contain the incoming shortwave flux at the TOA and instead the corresponding ERA-Interim field is used, which seems adequate since we consider only the mean climate state.

An overview of the observational reference datasets employed in this study is given in Table 2.

Both the satellite-derived radiation fields and the reanalysis fields were interpolated to a T42 grid and where possible, both all-sky and clear-sky fluxes were used. The period considered are the years 1990–99 for all the observational reference datasets. The land–sea mask applied to both model and observational data is the least common denominator of the different land–sea masks of the CMIP3 climate models, which were interpolated on a T42 grid.

c. Indices

Simple indices describing global climate change using surface air temperature patterns have been investigated in previous studies (Karoly and Braganza 2001). Braganza et al. (2003, 2004) examined the correlation structure of various indices and their internal variability during the twentieth century in the context of detection and attribution of climate change. The indices are chosen to capture and represent the spatial patterns of surface air temperature change due to the enhanced greenhouse effect. The key features of temperature change include the global temperature increase, larger warming over land than over ocean, greater warming at high latitudes than at low latitudes, a reduction in the magnitude of the annual cycle of temperature over land, and a difference in the warming between the Northern and Southern Hemisphere (NH and SH, respectively) arising from differences in the effects of aerosols and ocean mixing (Karoly and Braganza 2001). The indices, their definitions, and the abbreviations adopted in this paper are given in Table 3. Because of the similarities and mutual influence between temperature and radiation, the indices in this study were computed for all radiation variables, including surface and TOA fluxes. We introduce a new radiation variable called the ''atmospheric longwave absorption and emission variable,'' denoted in the following sections as α, which is simply the difference between the outgoing longwave radiation at the TOA ($LW\uparrow^{TOA}$) and the incoming longwave radiation at the surface ($LW\downarrow^{SFC}$). The corresponding shortwave attenuation variable, denoted by β, is the difference between the incoming solar radiation at the TOA ($SW\downarrow^{TOA}$) and the incoming shortwave radiation at the surface ($SW\downarrow^{SFC}$). An overview of the radiation variables employed in this study is listed in Table 4.

For a deeper insight into variations in space and surface types, the indices defined globally in Braganza et al. (2003) were computed separately here for land

TABLE 3. The indices, their definitions, and abbreviations used in this study.

Index	Definition	Abbreviation
Annual mean	The area-weighted AM radiation flux	AM
Land–ocean ratio	The ratio between the mean field over land and the mean field over ocean	LO
Interhemispheric difference	The difference between the mean NH field and the mean SH field	NS
Annual cycle	The magnitude of the AC was calculated for each hemisphere by subtracting the mean winter field from the mean summer field over land. These quantities were then area weighted by the fraction of global land surface area in the respective hemisphere and combined into a single index: $AC = w_{NH}(JJA - DJF) + w_{SH}(DJF - JJA)$	AC

TABLE 4. Definitions of symbols representing the shortwave, longwave, and net radiative fluxes for as and cs conditions as well as for cloud radiative forcing (crf).

Symbol	Definition
$LW\downarrow_{as}^{SFC}$	Downward longwave radiation at SFC for as conditions
$LW\downarrow_{cs}^{SFC}$	Downward longwave radiation at SFC for cs conditions
$LW\downarrow_{crf}^{SFC}$	Downward longwave radiation at SFC crf, equal to $LW\downarrow_{as}^{SFC} - LW\downarrow_{cs}^{SFC}$
$LW\uparrow_{as}^{SFC}$	Upward longwave radiation at the SFC for as conditions
$LW\uparrow_{as}^{TOA}, LW\uparrow_{cs}^{TOA}, LW\uparrow_{crf}^{TOA}$	Upward longwave radiation at TOA
$SW\downarrow_{as}^{SFC}, SW\downarrow_{cs}^{SFC}, SW\downarrow_{crf}^{SFC}$	Downward shortwave radiation at SFC
$SW\uparrow_{as}^{SFC}, SW\uparrow_{cs}^{SFC}, SW\uparrow_{crf}^{SFC}$	Upward shortwave radiation at SFC
$\Delta LW_{as}^{SFC}, \Delta LW_{cs}^{SFC}, \Delta LW_{crf}^{SFC}$	Net longwave radiation at SFC
$\Delta SW_{as}^{SFC}, \Delta SW_{cs}^{SFC}, \Delta SW_{crf}^{SFC}$	Net shortwave radiation at SFC
$\Delta_{as}^{SFC}, \Delta_{cs}^{SFC}, \Delta_{crf}^{SFC}$	Net radiation at SFC, equal to $\Delta SW + \Delta LW$
$\alpha_{as}, \alpha_{cs}, \alpha_{crf}$	Atmospheric longwave absorption and emission variable, equal to $LW\downarrow^{SFC} - LW\uparrow^{TOA}$
$\beta_{as}, \beta_{cs}, \beta_{crf}$	Atmospheric shortwave attenuation variable, equal to $SW\downarrow^{TOA} - SW\downarrow^{SFC}$

and ocean and were divided into zonal bands defined as follows: northern high latitudes (NH H: 90°–60°N), northern midlatitudes (NH M: 60°–30°N), northern tropics (NH T: 30°N–0°), southern tropics (SH T: 0°–30°S), southern midlatitudes (SH M: 30°–60°S), and southern high latitudes (SH H: 60°–90°S) where compatible with the definition that resulted in 50 indices. The indices were computed for the mean radiation of the period between the years 1990 and 1999. An overview of the indices used in this study to estimate climate sensitivity is shown in Fig. 1.

Both by definition and by chance, some of the indices are expected to be correlated. The 34 radiation variables and 50 indices for each of these radiation variables amount to a total of 1700 indices; thus, the correlation matrix has dimensions of 1700×1700 and cannot be visualized appropriately. An empirical orthogonal function (EOF) analysis of the correlation matrix—regarded as a spatial field—showed that 95% of the variance of the correlation matrix field can be explained by the first eight EOFs. On the one hand, this implies that the 1700 indices are highly correlated. On the other hand, the fact that at least eight EOFs are needed to explain most of the variance of the correlation matrix suggests that there is not a single pattern governing the correlations between all the indices.

d. Estimating climate sensitivity

The basic idea of this paper is illustrated in Fig. 1, where the indices for all radiation variables as computed by the CMIP3 multimodel set and their correlations to their corresponding climate sensitivities for the period 1990–99 are shown. The indices are not mutually independent, and the correlation coefficients vary from -0.89 to $+0.84$. We considered all correlations that are statistically significant at a 95% level. Three steps will lead to an estimate of climate sensitivity. First, a linear regression is carried out that determines the linear relationship between the index and the climate sensitivity. Subsequently, the quality of the linear relationship is quantitatively assessed via bootstrapping, giving a range of slopes between the radiative index and climate sensitivity. In the end, the index is computed for the eight observational datasets, which act as reference values. The intersection between the reference value and the bootstrapping sample gives a distribution of climate sensitivity for a particular index and a particular radiation variable.

The significance level of the correlation coefficient depends on the assumption of climate model independence. Previous studies noted that the CMIP3 multimodel ensemble constitutes an ''ensemble of opportunity'' rather than an independent set of models (Tebaldi and Knutti 2007; Knutti et al. 2010; Knutti 2010; Jun et al. 2008a,b). An example of this is the fact that some models are identical except for their resolution. Hence, the assumption of model independence is not correct. Therefore, we emphasize that the distributions of climate sensitivity estimates derived here cannot be regarded as proper probability distribution functions since the prerequisite of independence of both the climate models and the indices is not fulfilled in the framework of this study.

The idea of correlating an observable variable to a predicted quantity was illustrated, for example, by Hall and Qu (2006), where they examined the case of the snow albedo feedback and noticed that large intermodel variations in the snow albedo feedback strength in climate change are well correlated with comparably large intermodel variations in the feedback strength in the context of the seasonal cycle. The high correlation leads to the conclusion that eliminating the model errors in the seasonal cycle will directly lead to a reduction in the spread of feedback strength in climate change; hence, it has the ability to reduce the spread in simulations of the

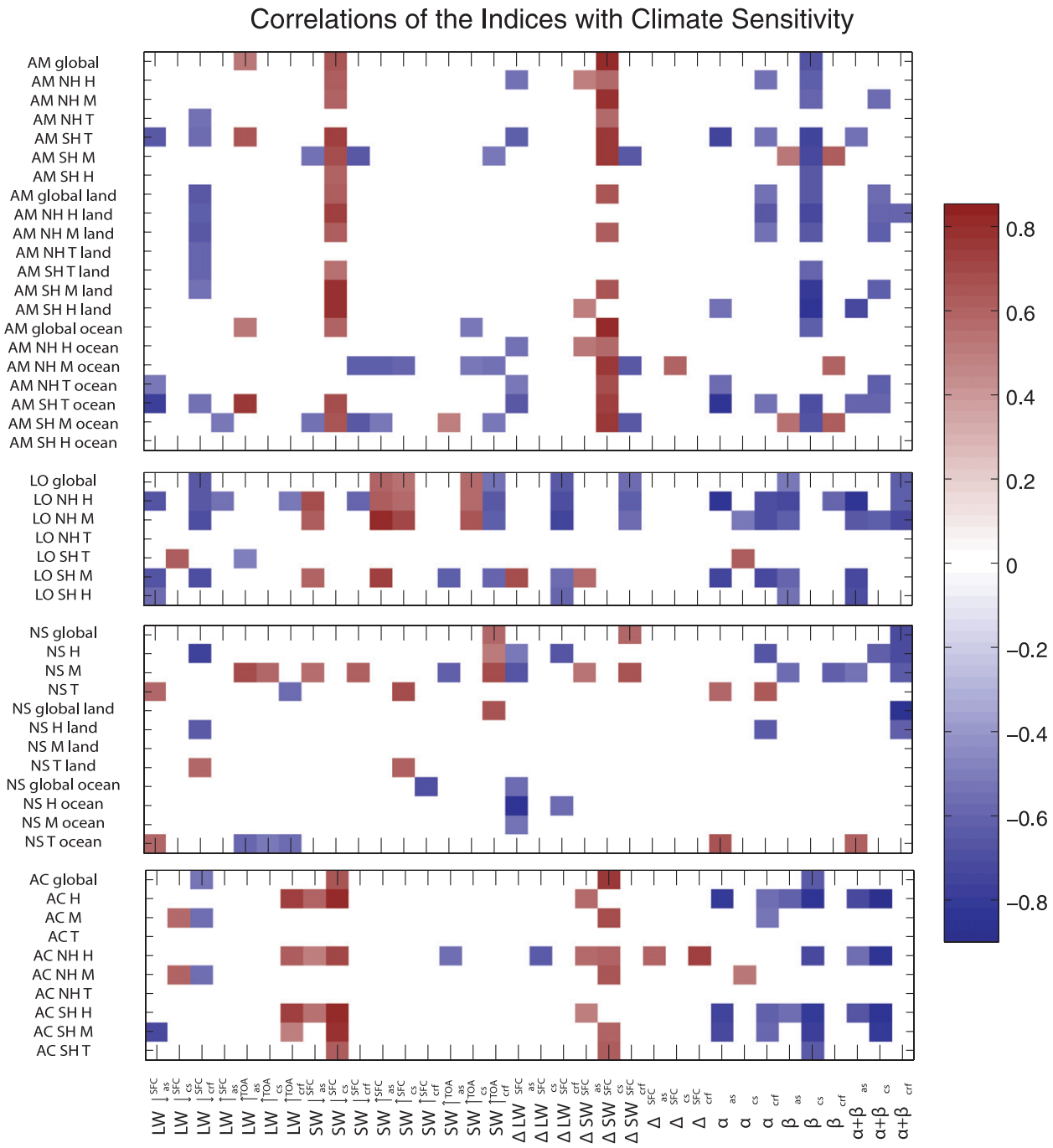

FIG. 1. Overview of the correlations between the indices (ordinate) for all radiation variables (abscissa) and the equilibrium climate sensitivities. The correlation coefficients are indicated in the color bar, and only the indices that are significant at a 95% level are shown. The indices were computed from the 1990 to 1999 climatology for the CMIP3 models (see text for details). The spatial grid was divided into zonal bands as defined in section 2 and separated into land and ocean. The symbols of the radiation variables are given in Table 4.

climate sensitivity, to the extent that snow cover feedbacks are a major driver of these differences. A similar approach was used to constrain climate sensitivity from the seasonal cycle in surface temperature (Knutti et al. 2006). Climate sensitivity was shown to relate to aspects of present-day climatology also in several other studies (Piani et al. 2005; Sanderson et al. 2008a,b). Sanderson et al. (2008a; see Fig. 7) in particular showed that current patterns of radiation provide a constraint on climate sensitivity in the Climateprediction.net ensemble.

The assumption here is that the correlation across models does not simply reflect the similarity of the models and uniformity of the underlying parameterizations but an intrinsic behavior resulting from physical processes. Of course this is difficult to prove, but support for that assumption is given by the fact that the CMIP3 models are structurally different (in contrast to the Climateprediction.net ensemble) and by the fact that the relations presented here can be understood in terms of physical processes. Moreover, the fact that high correlations are seen in different variables and regions and the consistency across the indices enhance the confidence in this method. Of course radiation indices can be changed in various ways, for example, by changing an albedo value of a land surface, which would probably not affect climate sensitivity. However, such changes are very likely to be random and uncorrelated across different models and would tend to weaken the observed correlation rather than spuriously introducing it. It is therefore very likely that the correlations indeed represent real variations in feedbacks. Note also that a strong correlation does not necessarily imply that the particular feedback is strong nor does it imply that it explains a large fraction of the climate sensitivity variation in CMIP3. A correlation may be strong, for example, in the high latitude, indicating a clear relation between the albedo feedback and climate sensitivity (Hall and Qu 2006) even though the spread in the albedo feedback is a relatively small contribution to the spread of the total feedback in the CMIP3 models (Soden and Held 2006).

3. Results

a. Relation of the radiative indices to clouds, atmospheric water vapor, and sea ice concentration

The radiative fluxes in the climate system are functions of its physical properties, for example, those of clouds, atmospheric water vapor, and sea ice concentration. Changes in these quantities can alter the radiative fluxes and induce radiative feedbacks that can dampen or amplify the initial perturbation. Here we show the indices defined above for the total cloud cover, the column-integrated amount of water vapor and sea ice concentration and correlate them to the radiative indices to relate particular indices to possible feedbacks that in turn can give insight into the correlations of the indices to climate sensitivity. These variables together with the relative humidity were used in a recent study by Fasullo (2010), who assessed the energy and water cycle feedbacks with respect to the land–ocean contrast.

The land–ocean contrast of clouds, water vapor, and sea ice is related to the land–ocean (LO) index of the radiation variables as shown Fig. 2. On a global level, we found that a high land–ocean contrast in total cloud cover in a model implies a high cloud radiative forcing (crf) for the incoming longwave radiation ($LW{\downarrow}_{crf}^{TOA}$) and the outgoing shortwave flux at the TOA ($SW{\uparrow}_{crf}^{TOA}$). In contrast, more clouds lead to less shortwave radiation reaching the surface ($SW{\downarrow}_{as}^{SFC}$). These relations can be explained by the absorptive and reflective properties of clouds. In the tropics, Fig. 2 indicates that a strong spatial land–ocean gradient in water vapor is related to a stronger clear-sky longwave surface flux ($LW{\downarrow}_{cs}^{SFC}$) over land than over ocean. The opposite is the case for the outgoing longwave flux at the TOA ($LW{\uparrow}_{as}^{TOA}$). The bottom panel of Fig. 2 illustrates that the sea ice concentration is positively correlated with the land–ocean contrast of the incoming all-sky and clear-sky shortwave surface radiation ($SW{\downarrow}_{as}^{SFC}$ and $SW{\downarrow}_{cs}^{SFC}$) because of the reflective properties of the sea ice surface. Overall, the correlations suggest that intermodel differences in physical properties and feedbacks induced by clouds, water vapor, and sea ice are at least partly reflected in the indices, even though a complete discussion of each of the hundreds of relations is not feasible.

b. Indices and correlations

Figure 1 illustrates the correlations between climate sensitivity and the 50 indices in the 34 radiation variables used in this study, which are significant at a 95% level. Since the CMIP3 dataset does not include clear-sky upward longwave fluxes at the surface, the net longwave cloud radiative forcing (ΔLW_{crf}^{SFC}) is approximated by $LW{\downarrow}_{cs}^{SFC} - LW{\uparrow}_{as}^{SFC}$. This approximation is also carried out for the reference datasets where possible. The correlation coefficients cover a range from -0.89 to $+0.84$, and we chose three of them in the following sections to illustrate the method of estimating climate sensitivity using a correlation between an observable radiative index and the climate sensitivity as computed by the CMIP3 models. The illustrative examples are cases where the correlation is significant and where the behavior can be understood in terms of known physical processes, that is, where the correlation is unlikely to be purely a statistical artifact resulting from calculating a large number of correlations.

Four radiation variables dominate the correlation structure in Fig. 1 by exhibiting significant correlations throughout most of the indices. These variables of interest are the cloud radiative forcing of the incoming longwave radiation at the surface $LW{\downarrow}_{crf}^{SFC}$, the clear-sky incoming shortwave flux $SW{\downarrow}_{cs}^{SFC}$, the net clear-sky shortwave surface budget ΔSW_{cs}^{SFC}, and the clear-sky atmospheric shortwave attenuation β_{cs}.

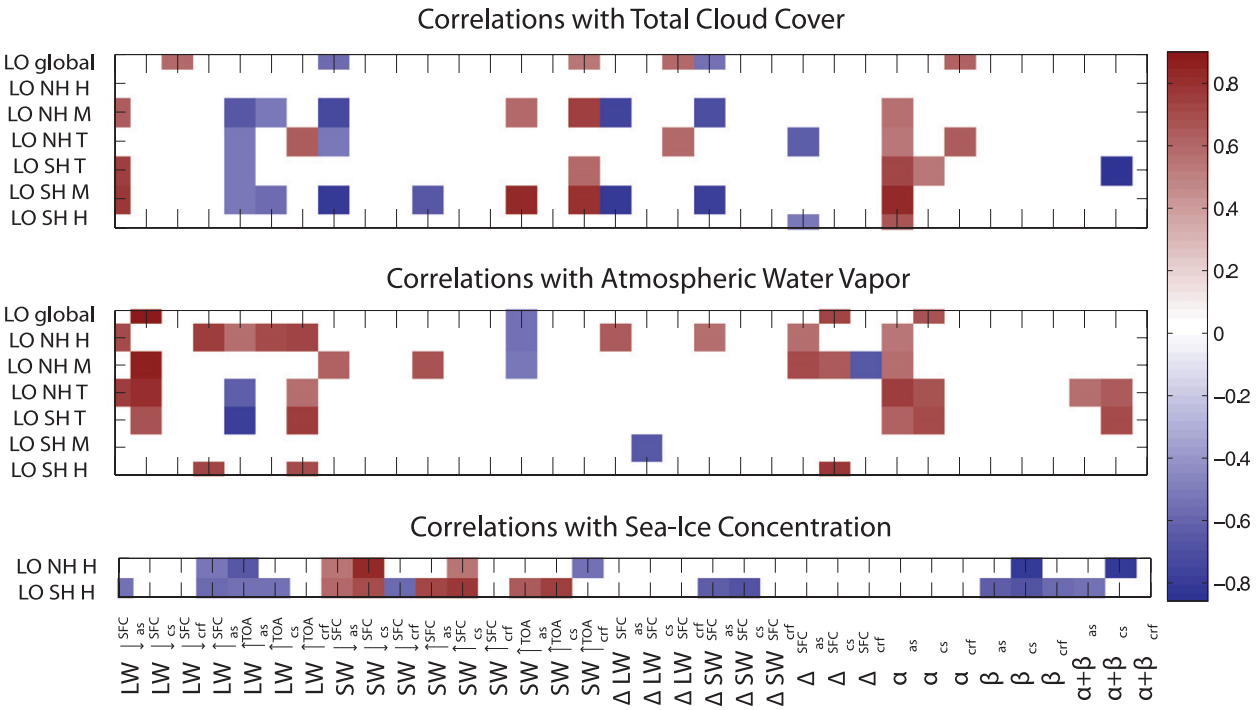

FIG. 2. Correlations of the LO indices of the radiation variables (ordinate) and the total cloud cover, the atmospheric water vapor, and sea ice concentration. The indices were computed for the mean state during the years 1950–99.

The regional partitioning of the indices highlight special regions of interest where correlations are apparent in almost all radiation variables, such as the southern tropics and southern midlatitudes along with the northern high latitudes. Some indices and their correlations appear to be governed by a particular kind of radiation—for example, the annual cycle index—mostly by the shortwave radiation, as can be seen at the bottom part of Fig. 1. The land–ocean index and the annual cycle index seem to represent useful indices to connect many radiation fluxes with climate sensitivity. Moreover, the atmospheric longwave absorption and emission variable α and atmospheric shortwave attenuation variable β feature significant correlations throughout almost all the indices, as shown in the right part of Fig. 1.

c. *Global indices*

The indices, their correlation coefficients to climate sensitivity, and the correlation structure among the indices are illustrated for the case of the global-mean indices as depicted in Fig. 3. The indices and their respective radiation variable are denoted in the bottom panel of Fig. 3 at the left-hand side of the symmetric correlation matrix. Red-colored blocks highlight positively correlated indices, whereas blue-shaded groups show negative correlations. The correlations of these indices with climate sensitivity are depicted in the top panel. Some of the correlations among different indices may appear by chance, whereas others result by definition of the indices; for example, it is assumed that for a given radiation variable, the annual-mean (AM) radiation over land is correlated with the global annual-mean radiation. This situation is clearly visible in the upper left corner of the correlation matrix where the annual mean indices in the $SW\downarrow_{cs}^{SFC}$ radiation for the entire globe (AM) and separately for land (AM land) and ocean (AM ocean) are highly correlated. Despite showing highly correlated indices, Fig. 3 also indicates that there are independent indices with white-colored blocks. Overall, the correlation matrix in Fig. 3 leads to the conclusion that the climate sensitivity estimates derived from the correlations of the indices in the top panel of Fig. 3 are not independent. Moreover, Fig. 3 can be used to infer the dominant fluxes in the radiation budgets of the surface and the atmosphere. Considering again the ''cluster'' of correlations in the AM index for the $SW\downarrow_{cs}^{SFC}$ radiation variable, Fig. 3 shows that by moving downward in the correlation matrix, it is the $SW\downarrow_{cs}^{SFC}$ flux that governs the same indices in β_{cs}.

We found that the annual-mean clear-sky shortwave radiation budget at the surface (AM $\times$ ΔSW_{cs}^{SFC}) is related to climate sensitivity with a correlation coefficient of $r = 0.84$. The same is true for the annual cycle in this radiation variable with $r = 0.76$. The correlation matrix

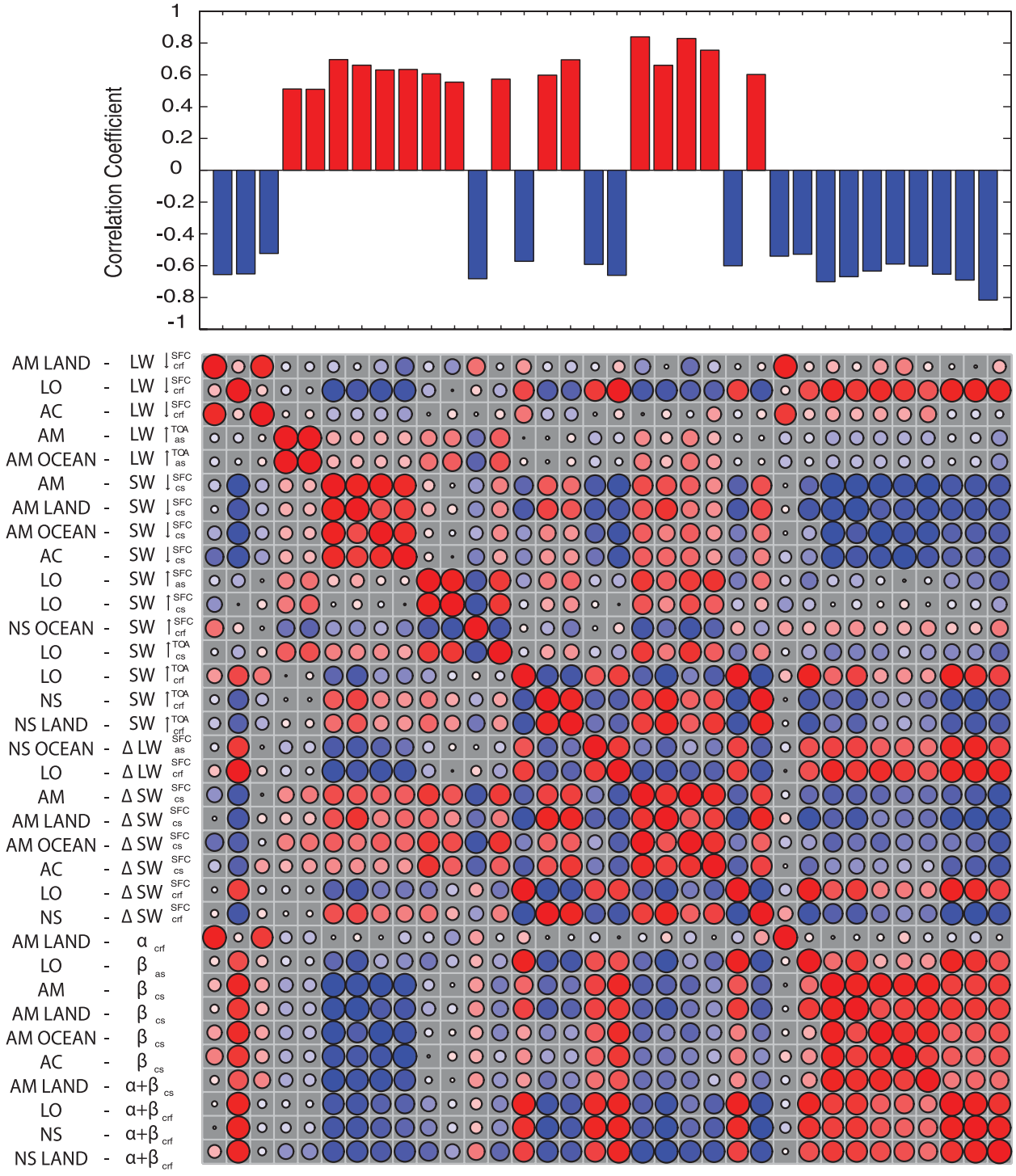

FIG. 3. Correlation coefficients of global indices with climate sensitivity that are significant at a 95% level are shown together with the correlation matrix of the indices. The size of the circles corresponds to the magnitude of the correlation. The red shading (blue circles) denotes positive (negative) correlation coefficients.

shows that these two indices are highly correlated. The ratio in the incoming cloud radiative forcing at the surface over land and ocean surfaces ($\mathrm{LO} \times \mathrm{LW}{\downarrow}_{\mathrm{crf}}^{\mathrm{SFC}}$) exhibits a correlation of $r = -0.65$ with climate sensitivity. This index is independent of the annual mean ($\mathrm{AM} \times \mathrm{LW}{\downarrow}_{\mathrm{crf}}^{\mathrm{SFC}}$), which is also correlated to sensitivity at $r = -0.66$.

d. Zonal partition of the indices

The zonal partition of the indices gives a spatial insight into the radiation patterns. Figure 4a shows the indices, the radiation variables, and correlations of the latter to climate sensitivity for the high latitudes. The land–ocean ratio index in the Northern Hemisphere is apparent throughout almost all shortwave and longwave radiation variables. A cluster of correlations is found for the annual cycle of the outgoing longwave radiation cloud radiative forcing at the TOA ($\mathrm{LW}{\uparrow}_{\mathrm{crf}}^{\mathrm{TOA}}$) and for both the all-sky and clear-sky incoming shortwave radiation at the surface ($\mathrm{SW}{\downarrow}_{\mathrm{as}}^{\mathrm{SFC}}$ and $\mathrm{SW}{\downarrow}_{\mathrm{cs}}^{\mathrm{SFC}}$). These correlations also govern similar correlations for the atmospheric absorption radiation variables α and β in the annual cycle (as seen in Fig. 4a).

Figure 4b depicts the correlation of the Northern Hemisphere land–ocean index of the all-sky incoming longwave surface radiation to climate sensitivity ($\mathrm{LO} \times \mathrm{LW}{\downarrow}_{\mathrm{as}}^{\mathrm{SFC}}$), the climate sensitivity estimates, and the relationship between the ($\mathrm{LO} \times \mathrm{LW}{\downarrow}_{\mathrm{as}}^{\mathrm{SFC}}$) index and the Northern Hemisphere LO index for the atmospheric water vapor. High sensitivity models tend to have a ($\mathrm{LO} \times \mathrm{LW}{\downarrow}_{\mathrm{as}}^{\mathrm{SFC}}$) index smaller than 1, implying that more longwave radiation reaches the ocean surfaces than the land surfaces in the northern high latitudes. These models have also a higher amount of water vapor above the oceans (as shown in the right panel of Fig. 4b). A higher amount of water vapor leads to an enhanced atmospheric absorption of longwave radiation; hence, the correlation between the ($\mathrm{LO} \times \mathrm{LW}{\downarrow}_{\mathrm{as}}^{\mathrm{SFC}}$) index and climate sensitivity can be partly attributed to the longwave water vapor feedback. The comparison with the reference datasets suggests that high sensitivity models capture the ($\mathrm{LO} \times \mathrm{LW}{\downarrow}_{\mathrm{as}}^{\mathrm{SFC}}$) index better and that the climate sensitivity estimates are between 2.7 and 4.5 K.

The correlations of the indices in the midlatitudes with climate sensitivity are depicted in Fig. 5a. In the longwave regime, the cloud radiative forcing of the incoming longwave radiation at the surface ($\mathrm{LW}{\downarrow}_{\mathrm{crf}}^{\mathrm{SFC}}$) shows negative correlations with climate sensitivity in the annual mean over land ($r = -0.66$), the land–ocean index ($r = -0.70$), and in the annual cycle index ($r = -0.55$). Strong negative correlations are found in the atmospheric longwave variable a for the land–ocean ratio. The relationship between the interhemispheric difference in the midlatitudes for the outgoing longwave at the TOA ($\mathrm{NS} \times \mathrm{LW}{\uparrow}_{\mathrm{as}}^{\mathrm{TOA}}$) to climate sensitivity and the same index for total cloud cover is shown in Fig. 5b. High-sensitivity models show more longwave radiation escaping the TOA in the northern midlatitudes, whereas the low-sensitivity model features the opposite. The correlation coefficient between the ($\mathrm{NS} \times \mathrm{LW}{\uparrow}_{\mathrm{as}}^{\mathrm{TOA}}$) index to its respective cloud cover index is $r = -0.84$ and implies that the more clouds the models compute for the southern midlatitudes, the more longwave radiation is trapped in the climate system and the higher the ($\mathrm{NS} \times \mathrm{LW}{\uparrow}_{\mathrm{as}}^{\mathrm{TOA}}$). Thus, the intermodel differences in the longwave cloud feedback can be partly attributed to the correlation of the ($\mathrm{NS} \times \mathrm{LW}{\uparrow}_{\mathrm{as}}^{\mathrm{TOA}}$) index to climate sensitivity.

In the tropics, most correlations of the indices with climate sensitivity are found for the AM index, as illustrated in Fig. 6. The AC index shows almost no correlations. The dominating radiation variables are $\mathrm{LW}{\downarrow}_{\mathrm{as}}^{\mathrm{SFC}}$, $\mathrm{LW}{\downarrow}_{\mathrm{crf}}^{\mathrm{SFC}}$, $\mathrm{LW}{\uparrow}_{\mathrm{as}}^{\mathrm{TOA}}$, and $\mathrm{SW}{\downarrow}_{\mathrm{cs}}^{\mathrm{SFC}}$. The strong correlations in these radiation variables also induce strong correlations in the net and atmospheric radiation budgets, which include the former variables. Figure 6 also highlights that it is the annual-mean radiation in the ocean, and in general the radiation variables above the ocean, that exhibits the most numerous correlations to climate sensitivity.

The annual-mean all-sky outgoing longwave flux at the TOA in the southern ocean is correlated to climate sensitivity with a correlation coefficient of $r = 0.77$, as shown in Fig. 6b). The same flux is also negatively correlated to the total cloud cover in the southern tropical oceans, implying that a high cloud cover increases the amount of longwave radiation in this area. This relationship suggests that high-sensitivity models generally have a low total cloud cover in the southern oceans and thus emit more longwave radiation into space. In this framework, the positive correlations of the clear-sky incoming surface shortwave radiation to climate sensitivity could neither be related to the total cloud amount nor the atmospheric water vapor.

e. Climate sensitivity estimates

In total, we found that 276 radiative indices correlated with climate sensitivity at a 95% significance level during the period 1990–99. The correlations among the indices, as shown in Fig. 3, imply that the climate sensitivity estimates are mutually dependent as well. To account for uncertainty in the linear regression between the index and climate sensitivity, we computed a sample of 1000 bootstrapping estimates of the errors of the

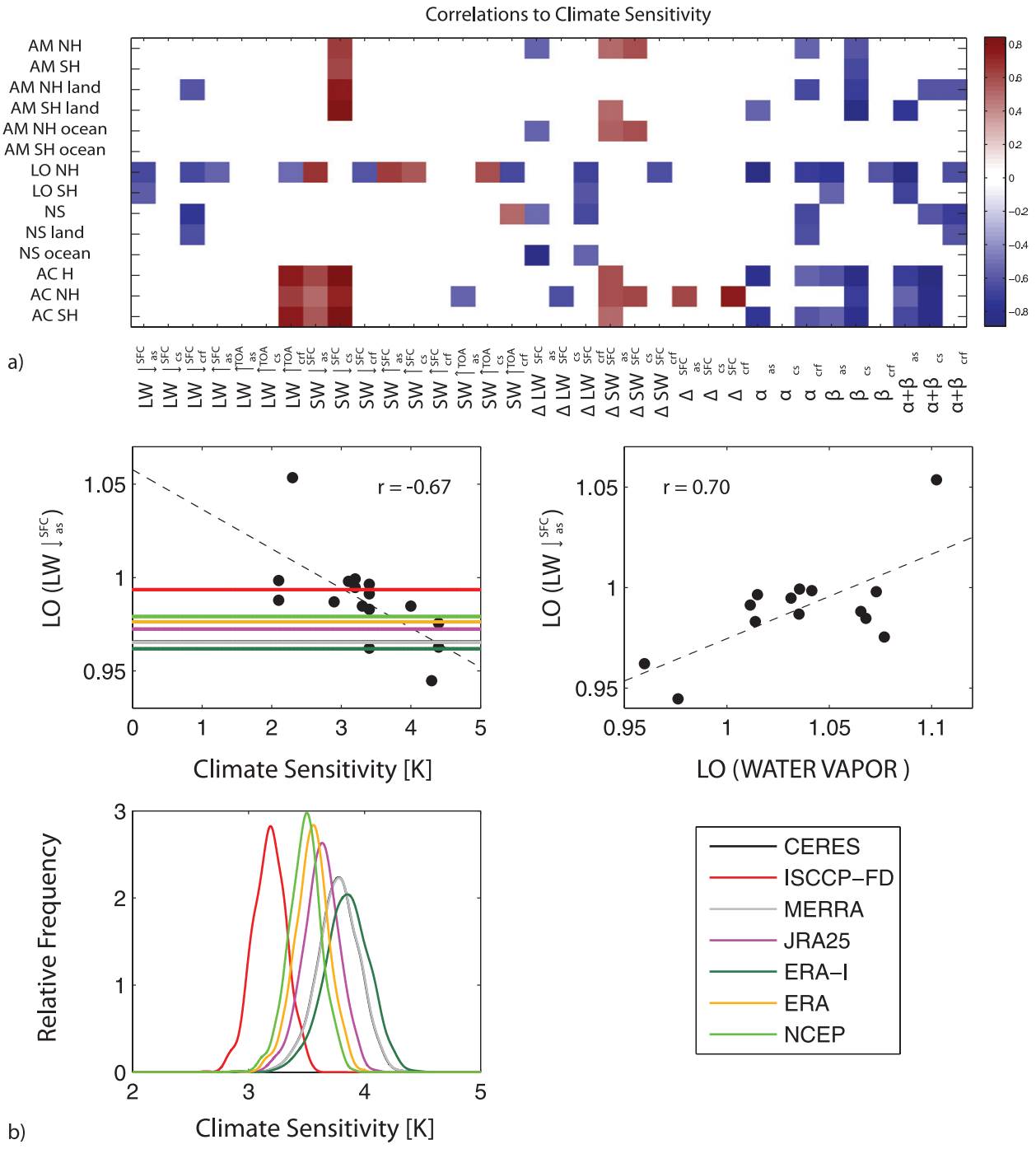

FIG. 4. (middle) Illustrative examples of the correlations between (left) a radiative index and the equilibrium climate sensitivity computed by the CMIP3 models for the high latitudes and (right) the correlation of the same index for the particular radiation variable of the left panel and the water vapor variable. (top) The particular index is indicated on the ordinate and the radiation variables are shown on the abscissa. (bottom) The kernel density estimates for climate sensitivity derived by bootstrapping and comparison of the linear relation between a radiative index and climate sensitivity with the observational reference datasets.

coefficient vector in the linear regression. This results in 276 000 climate sensitivity estimates for each reference dataset (the number is smaller where not all radiation fields were available). The kernel density estimates for the eight reference datasets are depicted in Fig. 7. The distributions must not be regarded as probability distribution function of climate sensitivity because of the dependencies of the indices.

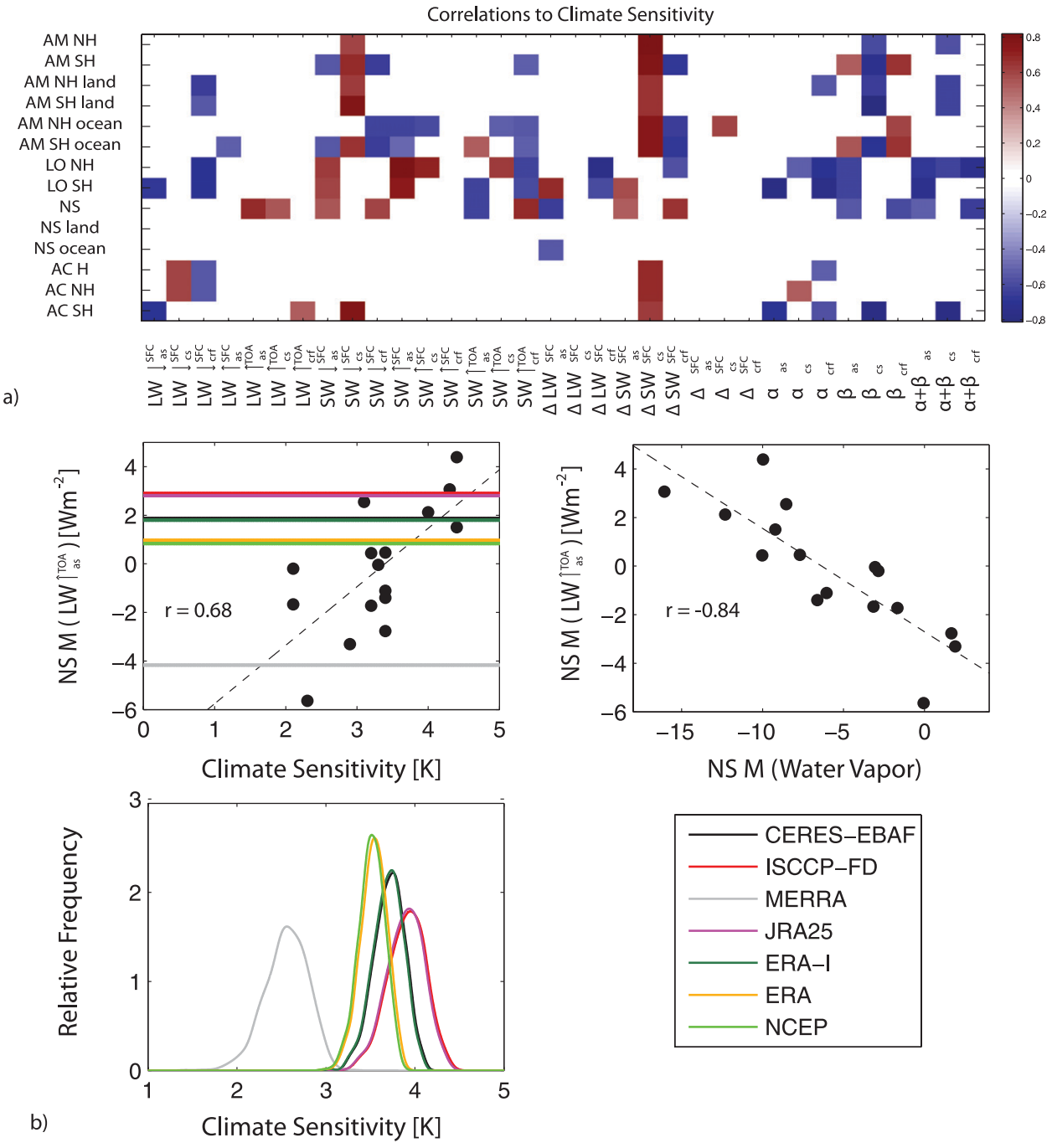

FIG. 5. As in Fig. 4, but for the midlatitudes.

The climate sensitivity was estimated from the mean of the indices during the years 1990–99 for the CMIP3 models and the 5-yr climatology of the CERES and CERES EBAF data. For the best-guess estimate of climate sensitivity, we take the median of the kernel density distribution, resulting in a best guess of 3.3 (CERES), 3.3 (ERBE), 3.5 (MERRA), 3.4 (ERA-Interim), 3.6 (JRA-25), 3.5 (ERA-40), 3.6 (NCEP), and 3.3 K (ISCCP-FD). The corresponding likely ranges are taken as the 66% ranges of the kernel density distributions and are 2.7–4.0 (CERES), 1.7–3.8 (ERBE), 2.8–4.1 (MERRA), 2.7–3.9 (ERA-Interim), 3.0–4.2 (JRA-25), 3.0–4.0 (ERA-40), 3.1–4.7 (NCEP), and 2.9–3.7 K for the ISCCP-FD dataset. Aggregating the climate sensitivity estimates of the

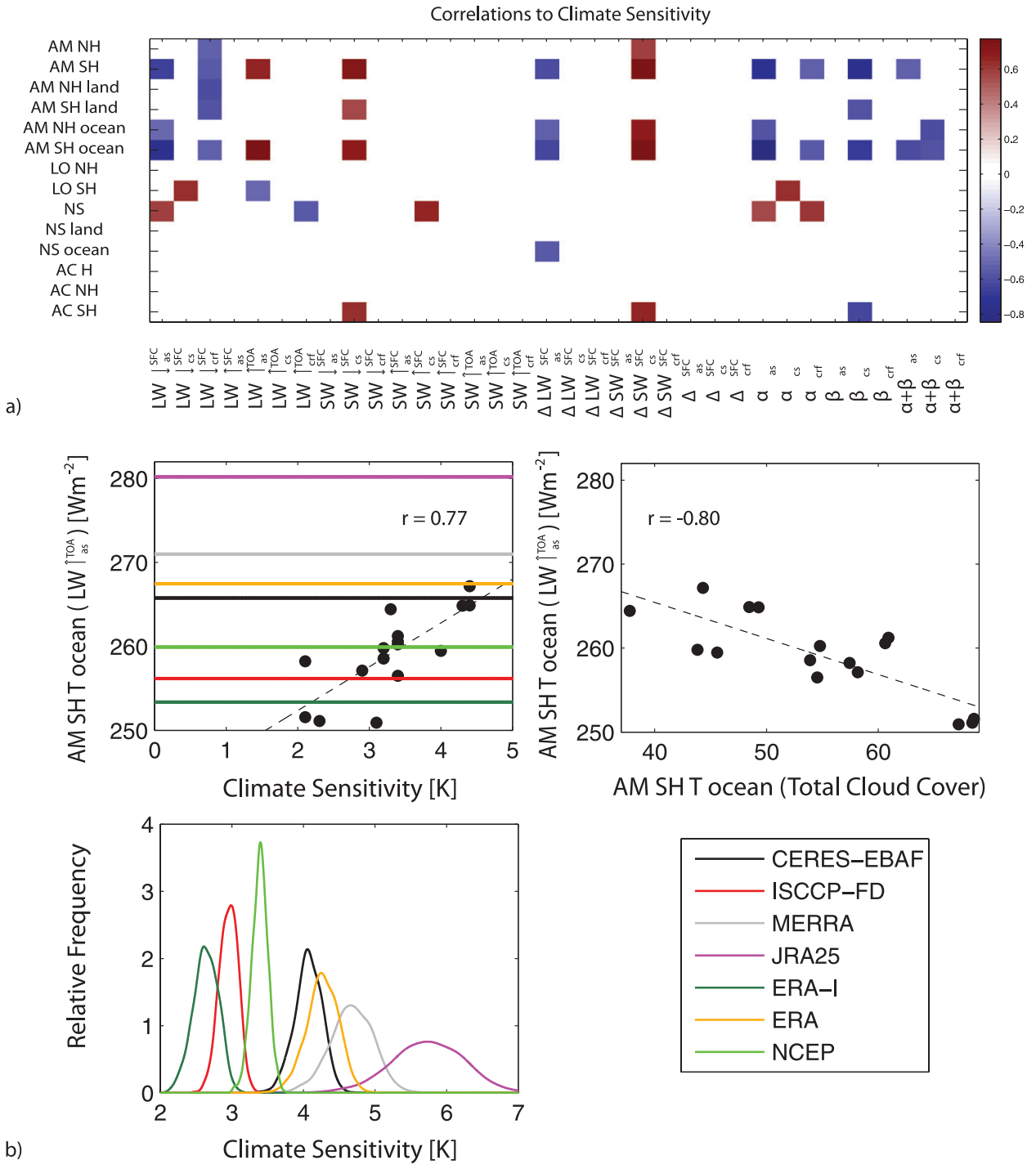

FIG. 6. As in Fig. 4, but for the tropics.

individual observational reference datasets into one sample, the best estimate of climate sensitivity is 3.4 K with a likely range of 2.9–4.0 K.

The bottom panel of Fig. 7 compares the likely ranges with the corresponding range of 2–4.5 K estimates by the IPCC. All estimates lie within the IPCC range except for the NCEP reanalysis, with an upper range slightly exceeding 4.5 K and the ERBE dataset with a slightly lower range. The distribution of the ERBE-derived estimates contains only TOA fluxes and has

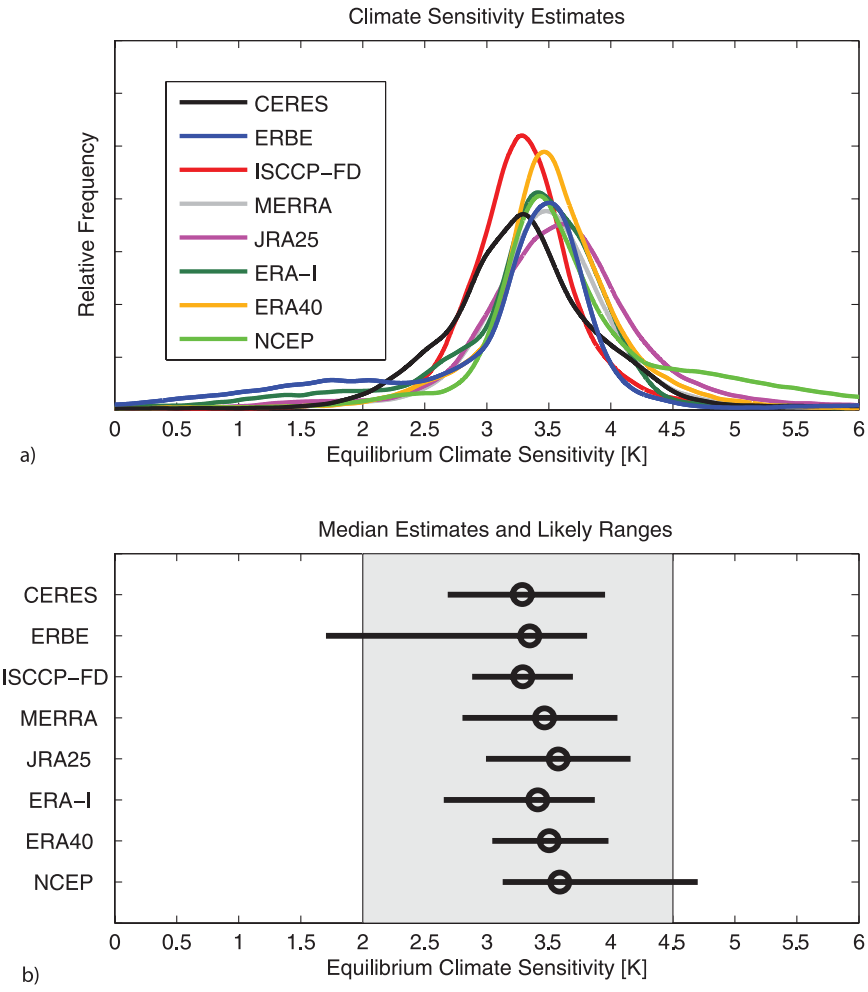

FIG. 7. (a) Kernel density estimates for climate sensitivity for various observational reference datasets. Distributions were computed using a bootstrapping sample of a linear regression between a radiative index and climate sensitivity where the correlation is significant at a 95% level. Because of different data availability among the reference datasets, the size of bootstrapping samples varies among the kernel density estimates. (b) Depiction of the median and 66% likely ranges.

because of its lower amount of correlations, a broader range than estimates derived from both surface and TOA data. For individual reference datasets, Fig. 7 indicates that values for the sensitivity below 1.7 K are not likely to be consistent with current observed radiation patterns within the framework of our method. This lower bound increases to 2.9 K if we aggregate the reference datasets, whereas values exceeding 4.5 K cannot be excluded from our analysis, but they are rather unlikely and appear less likely than those found, for example, in the Climateprediction.net (Stainforth et al. 2005). While these ranges cannot be interpreted properly in terms of probability, they are consistent with other estimates of climate sensitivity (Knutti and Hegerl 2008).

4. Discussion

A variety of uncertainties arises in every step of our procedure. Parametric and systematic uncertainties in the CMIP3 multimodel ensemble cause errors in the radiative fluxes and thus in the radiative indices computed in this study. Moreover, the models share similar deficiencies and may not cover the full model space (Tebaldi and Knutti 2007). Additionally, the eight observational datasets feature similar deficiencies and should not be regarded as mutually independent reference datasets. The method of deriving an estimate of climate sensitivity using a correlation of climate model patterns highly depends on the value inferred from the observational

datasets, which in turn crucially depends on the uncertainty of the linear regression. Hence, the estimates of climate sensitivity are sensitive to structural biases in the observational datasets, either derived from reanalyses or satellite products, and to the correlation coefficient. Some of the issues are discussed in more detail below.

The uncertainty in the linear regression was quantitatively assessed by computing a bootstrapping sample with 1000 estimates for each correlation. The indices chosen in this study are not mutually independent, as the correlation matrix for the globally defined indices in Fig. 3 shows. Moreover, Huybers (2010) noted physically unexpected correlations among different feedbacks in the CMIP3 climate models that may arise from tuning and compensating errors in models. Hence, it is not possible in the framework of this study to quantitatively relate a particular index and its correlation to climate sensitivity to a particular feedback process in a climate model. By computing the indices defined here for the total cloud cover, the atmospheric water vapor, and the sea ice concentration in the model, we could show that intermodel differences in one of these quantities are related to the radiative indices and highlight the physical properties, such as the radiative absorption and reflectivity of clouds. Thus, we conclude that the radiative indices employed in this study are related to physical feedbacks, which in turn influence climate sensitivity.

The indices used in this study were in initially place temperature-based and employed by Braganza et al. (2003, 2004) in a detection and attribution framework in the context of climate change. The usage of the indices as a predictor for climate sensitivity reflects the assumption that the radiative indices and their spatial distribution give insight into the radiative feedbacks and physical processes underlying the radiation patterns. The link between radiation fields and climate feedbacks has been previously assessed by the computation of radiative kernels both in multimodel and perturbed physics ensembles (Soden et al. 2008; Sanderson et al. 2009). Spatial indices of cloud amount were also shown to correlate with climate sensitivity. Volodin (2008) examined the cloud amount of the CMIP3 models and found a correlation of $r = -0.82$ between the equilibrium climate sensitivity and the residual of cloud amount of the tropics (28°S–28°N) and southern temperate latitudes (56°–36°S). Hence, it is natural to assume that there are also spatial indices in the radiation variables itself, which are directly affected by the cloud amount and being related to the equilibrium climate sensitivity. Previous studies examined physical processes, such as the land–ocean contrast (Sutton et al. 2007; Joshi et al. 2008) and the polar amplification (Holland and Bitz 2003), primarily for the temperature variable. Recently, Fasullo (2010) found that land–ocean contrasts in radiative fluxes and cloud amount in CMIP3 climate model ensemble are crucial in the way the energy budget equilibrates in response to forcing. This study attempts to give some insights into these processes for the various radiation fluxes in the climate system in a qualitative way.

The zonal partitioning of the indices is designed to highlight different regions in which particular indices are related to climate sensitivity. Figure 6 shows that the indices both in the annual-mean longwave and shortwave radiation in the southern ocean are correlated to climate sensitivity. Bony and Dufresne (2005) found that differences in the marine boundary layer clouds are to a great extent responsible for cloud feedback uncertainties in the tropics. Studying the energy budget of the southern ocean, Trenberth and Fasullo (2010) found that errors in the energy budget of the Southern Hemisphere are negatively correlated to the equilibrium climate sensitivity. The correlation of $r = -0.73$ of the model sensitivity to the net downward flux at the TOA might be linked to the negative biases in cloud amount, which are together with cloud type, cloud-top height, and radiative properties one of the main reasons for the differences of TOA radiation between climate models and satellite measurements (Trenberth and Fasullo 2010).

A variety of studies investigated the radiative effects of clouds and their impact on climate (e.g., Arking 1991; Vavrus 2004; Stephens 2005; Soden and Held 2006). The fact that correlations between the radiative indices and climate sensitivities are found both in full-sky and clear-sky fluxes, as shown in Fig. 1, highlight the influence of clouds on the radiation budget and on climate sensitivity. To account for the effect of different cloud types and other climate variables on the indices and thereby on our estimates of climate sensitivity, an extended analysis including diagnostics, for example, from the vertical pressure velocity (Bony and Dufresne 2005) and the distinction between low- and high-cloud fraction (Karlsson et al. 2008) would have to be included in our analysis.

The climate sensitivity estimates derived here crucially depend on the accuracy of the reference datasets. To assess this sort of uncertainty, we employed various satellite-derived datasets and reanalysis-based data. At the TOA, satellite data generally performs better than other types of data, such as reanalyses (Trenberth et al. 2009). A comprehensive illustration and computation of the current best estimates of global energy flows in the climate system by comparing different satellite and reanalysis data is given by Trenberth et al. (2009). Their results are mainly based on new measurement of CERES instruments. Other satellite-derived

datasets, such as the ISCCP-FD project, exhibit uncertainties of 10–15 W m^{-2} at the surface and 5–10 W m^{-2} at the TOA as well as spurious trends and discontinuities (Zhang et al. 2004; Dai et al. 2006). Trenberth et al. (2009) compared the ERA-40, the NCEP reanalysis, and the ISCCP-FD dataset and noted significant deficiencies and biases. The imbalance at the TOA between the energy absorbed and emitted by the climate system is measured by satellite data to be between −3 and 7 W m^{-2} (Loeb et al. 2009), while the current best estimate by Hansen et al. (2005) is 0.85 ± 0.15 W m^{-2}. Loeb et al. (2009) note that that this discrepancy is due to uncertainties in absolute calibration and algorithms. Thus, we used a modified CERES data that matches the TOA imbalance computed by Hansen et al. (2005). Fasullo and Trenberth (2008) used this adjustment to compute the annual cycle of the energy budget of the climate system.

In a comparison of the ERA-40 and NCEP–NCAR near-surface datasets, Betts et al. (2006) found differences in the climatologies of the two different datasets along with consistent and coherent patterns of the major seasonal anomaly fields. They exhibit warm and dry seasonal biases associated with reduced precipitation and cloudiness. Prior studies noticed some deficiencies in the all-sky radiation at the TOA because of the inaccurate representation of cloud radiative properties (Allan et al. 2004). Based on their observations from multiple satellite instruments, Allan et al. (2004) conclude that the all-sky radiation budget simulated by ERA-40 displays large systematic biases. Despite deficiencies in the all-sky radiation budget, the clear-sky radiation budget simulated by ERA-40 compares well with independent satellite data (Allan et al. 2004; Uppala et al. 2005).

When comparing the climate models to observations, one has to consider the fact that the model development involved some tuning toward the current climate. Hence, it is likely that the observations often fall within the range of the model indices. For example, Trenberth and Fasullo (2010) note that energy and moisture are conserved to order 1 W m^{-2} by the models. In an experiment where the Community Atmosphere Model, version 3 (CAM3) is tuned to fit the TOA energy budget of the ERBE and CERES data, Bender (2008) found that the climate sensitivity resulting from the two-tuned version differed by 0.24 K, which is much smaller than the differences in the CMIP3 multimodel set. Because of the particular definitions of the indices, both in terms of space (e.g., the zonal slice ''northern midlatitudes'') and processes (e.g., the land–ocean contrast), we argue that is not possible to tune exactly these indices of the models toward observations, since most model calibration efforts focus on global-mean values, for example, on the global-mean energy budget by adjusting the albedo- or cloud-related properties. Moreover, the use of eight different reference datasets—some of them have just recently become public (e.g., MERRA)—enhances the confidence that the model-based indices can be at least partly regarded as independent of the observational datasets.

Despite the uncertainties mentioned above, the consistency of the estimates across different indices and eight reference datasets, as shown in Fig. 7, suggests that the range of climate sensitivity derived with the method of this study is robust. Because of the mutual correlations among the indices, some climate sensitivity estimates are accounted for several times, suggesting that the ranges depicted in Fig. 7 are likely to be underestimated, although the best guess of 3.4 K for climate sensitivity when the reference datasets are aggregated appears to constitute a robust quantity.

5. Conclusions

Climate change manifests itself in the perturbation of the earth's radiation balance; hence, the accurate representation of the radiative fluxes in the climate system is a prerequisite of any climate model and observational datasets. We use indices of spatial radiation patterns to highlight both intermodel differences in modeling radiation in the group of CMIP3 models and their relation to the equilibrium climate sensitivity. Particular regions of interest are highlighted where these intermodel differences correlate to the climate sensitivity, such as the southern tropical oceans or the high latitudes. While the correlations represent a pure statistical tool to constrain both radiation fields and climate sensitivity, the behavior in different regions give insight into the possible effects of feedback processes, which are the source of uncertainty with respect to the climate sensitivity, especially the cloud feedback. Correlations between the climate sensitivity and the radiative indices are found both in all-sky and clear-sky fluxes, particularly in the tropical regions, emphasizing the importance of accurate clear-sky and cloud related feedback parameterization. These findings go along with previous studies that noted the link between the radiative properties of clouds and the climate (Arking 1991; Bony et al. 2004; Vavrus 2004; Stephens 2005; Soden and Held 2006; Volodin 2008).

Despite biases and deficiencies in the observational reference datasets, the analysis supports a value for climate sensitivity in the range of 2.5–5 K, and furthermore that climate sensitivities below 1.7 K are not likely to be consistent with observed radiation patterns in the

current climate model structure based on individual observational reference datasets. Aggregating the eight reference datasets, we derive a likely range of climate sensitivity of 2.9–4.0 K with a median estimate of 3.4 K in agreement with previous studies that estimated the lower tail of climate sensitivity using the perturbed physics approach by Climateprediction.net. Those studies found a 5%–95% probability range of 2.4–5.4 K (Murphy et al. 2004), 2.2–6.8 K (Piani et al. 2005), and a frequency distribution of the simulated climate sensitivity that ranges from 1.9 to 11.5 K (Stainforth et al. 2005). They stress that few model versions have sensitivities less than 2 K, whereas the long tail extends to very high values. Overall, the studies highlight the low probability of a climate sensitivity below 2 K. Various methods have been derived to constrain climate sensitivity, and an overview of their probability distribution functions are depicted in Fig. 3 of Knutti and Hegerl (2008). While the range and number of probability distribution functions are large, most studies are consistent in their best estimate, with the average of 3.3 K computed by the CMIP3 multimodel ensemble (Meehl et al. 2007), along with 3.3 (Piani et al. 2005), 3.4 (Stainforth et al. 2005), and between 3 and 3.5 K Knutti et al. (2006) for the CPDN-perturbed physics ensemble. Our mean estimate of 3.4 K for the climate sensitivity fits well in this list.

The limitation here is that the number of models is rather small. On the other hand, a correlation across structurally different models is less likely to be an artifact of an oversimplified parameterization, as it may happen in a perturbed physics ensemble. The results therefore provide strong support for the lower bound of climate sensitivity seen in the CPDN ensemble; however, in contrast to those earlier studies, they are not conditional on a Hadley Centre model structure. Because of the correlation of some variables, the estimates of the climate sensitivity cannot be regarded as mutually independent. Additionally, our indices do not cover the entire space of possible correlations, for example, because of the motivated but still arbitrary zonal partitioning of the indices. Noting the range of the bias field, an improvement of the radiation fields in reanalysis datasets would better constrain climate sensitivity.

The spread of the indices highlight the need for an adequate representation of the radiation patterns in the global climate system. Our method constitutes a first, simple approach to constrain the climate sensitivity using a variety of radiation variables. While the concept of the climate sensitivity is a global approach, the computation of regional climate sensitivities could facilitate the investigation of the influence of physical feedback processes on climate sensitivity (Boer and Yu 2003). The results of this study, particularly the derived sensitivity, should be regarded with some caution, given the biases and deficiencies in the CERES, ERBE, ISCCP-FD, MERRA, JRA-25, ERA-Interim, ERA-40, and NCEP datasets. Nevertheless, the results reaffirm that the present-day climatology provides a strong constraint on the lower bound of climate sensitivity in the current structure of GCMs.

Acknowledgments. We acknowledge the modeling groups the Program for Climate Model Diagnosis and Intercomparison (PCMDI) and the WCRP's Working Group on Coupled Modelling (WGCM) for their roles in making available the WCRP CMIP3 multimodel dataset. Support of this dataset is provided by the Office of Science, U.S. Department of Energy. We thank Y.-C. Zhang of NASA's Goddard Institute for Space Studies for data and support. The research of Dr. J. Fasullo is sponsored by NASA under Grant NNX09AH89G.

REFERENCES

Allan, R. P., M. A. Ringer, J. A. Pamment, and A. Slingo, 2004: Simulation of the earth's radiation budget by the European Centre for Medium-Range Weather Forecasts 40-year reanalysis (ERA40). *J. Geophys. Res.,* **109,** D18107, doi:10.1029/2004JD004816.

Allen, M., and Coauthors, 2006: Observational constraints on climate sensitivity. *Avoiding Dangerous Climate Change,* H. J. Schellnhuber et al., Eds., Cambridge University Press, 281–289.

Arking, A., 1991: The radiative effects of clouds and their impact on climate. *Bull. Amer. Meteor. Soc.,* **72,** 795–813.

Bender, F. A. M., 2008: A note on the effect of GCM tuning on climate sensitivity. *Environ. Res. Lett.,* **3**.

Betts, A. K., M. Zhao, P. A. Dirmeyer, and A. C. M. Beljaars, 2006: Comparison of ERA40 and NCEP/DOE near-surface data sets with other ISLSCP-II data sets. *J. Geophys. Res.,* **111,** D22S04, doi:10.1029/2006JD007174.

Boer, G. J., and B. Yu, 2003: Climate sensitivity and response. *Climate Dyn.,* **20,** 415–429.

Bony, S., and J.-L. Dufresne, 2005: Marine boundary layer clouds at the heart of tropical cloud feedback uncertainties in climate models. *Geophys. Res. Lett.,* **32,** L20806, doi:10.1029/2005GL023851.

——, ——, H. Le Treut, J. J. Morcrette, and C. Senior, 2004: On dynamic and thermodynamic components of cloud changes. *Climate Dyn.,* **22,** 71–86.

Braganza, K., D. J. Karoly, A. C. Hirst, M. E. Mann, P. Stott, R. J. Stouffer, and S. F. B. Tett, 2003: Simple indices of global climate variability and change: Part I –Variability and correlation structure. *Climate Dyn.,* **20,** 491–502.

——, ——, ——, P. Stott, R. J. Stouffer, and S. F. B. Tett, 2004: Simple indices of global climate variability and change. Part II: Attribution of climate change during the twentieth century. *Climate Dyn.,* **22,** 823–838.

Cess, R. D., and Coauthors, 1989: Interpretation of cloud-climate feedback as produced by 14 atmospheric general circulation models. *Science,* **245,** 513–516.

Dai, A., T. R. Karl, B. Sun, and K. E. Trenberth, 2006: Recent trends in cloudiness over the United States: A tale of monitoring inadequacies. *Bull. Amer. Meteor. Soc.,* **87,** 597–606.

Dufresne, J. L., and S. Bony, 2008: An assessment of the primary sources of spread of global warming estimates from coupled atmosphere–ocean models. *J. Climate,* **21,** 5135–5144.

Fasullo, J. T., 2010: Robust land–ocean contrasts in energy and water cycle feedbacks. *J. Climate,* **23,** 4677–4693.

——, and K. E. Trenberth, 2008: The annual cycle of the energy budget. Part I: Global mean and land–ocean exchanges. *J. Climate,* **21,** 2297–2312.

Forest, C. E., P. H. Stone, A. P. Sokolov, M. R. Allen, and M. D. Webster, 2002: Quantifying uncertainties in climate system properties with the use of recent climate observations. *Science,* **295,** 113–117.

Gregory, J. M., and Coauthors, 2004: A new method for diagnosing radiative forcing and climate sensitivity. *Geophys. Res. Lett.,* **31,** L03205, doi:10.1029/2003GL018747.

Hall, A., and X. Qu, 2006: Using the current seasonal cycle to constrain snow albedo feedback in future climate change. *Geophys. Res. Lett.,* **33,** L03502, doi:10.1029/2005GL025127.

Hansen, J., and Coauthors, 2005: Earth's energy imbalance: Confirmation and implications. *Science,* **308,** 1431–1435.

Harvey, L. D. D., and R. K. Kaufmann, 2002: Simultaneously constraining climate sensitivity and aerosol radiative forcing. *J. Climate,* **15,** 2837–2861.

Holland, M. M., and C. M. Bitz, 2003: Polar amplification of climate change in coupled models. *Climate Dyn.,* **21,** 221–232.

Huybers, P., 2010: Compensation between model feedbacks and curtailment of climate sensitivity. *J. Climate,* **23,** 3009–3018.

Joshi, M. M., J. M. Gregory, M. J. Webb, D. M. H. Sexton, and T. C. Johns, 2008: Mechanisms for the land/sea warming contrast exhibited by simulations of climate change. *Climate Dyn.,* **30,** 455–465.

Jun, M., R. Knutti, and D. W. Nychka, 2008a: Local eigenvalue analysis of CMIP3 climate model errors. *Tellus,* **60A,** 992–1000.

——, ——, and ——, 2008b: Spatial analysis to quantify numerical model bias and dependence: How many climate models are there? *J. Amer. Stat. Assoc.,* **103,** 934–947.

Kalnay, E., and Coauthors, 1996: The NCEP/NCAR 40-Year Reanalysis Project. *Bull. Amer. Meteor. Soc.,* **77,** 437–471.

Karlsson, J., G. Svensson, and H. Rodhe, 2008: Cloud radiative forcing of subtropical low level clouds in global models. *Climate Dyn.,* **30,** 779–788.

Karoly, D. J., and K. Braganza, 2001: Identifying global climate change using simple indices. *Geophys. Res. Lett.,* **28,** 2205–2208.

Knutti, R., 2010: The end of model democracy? *Climatic Change,* **102,** 395–404, doi:10.1007/s10584-010-9800-2.

——, and G. C. Hegerl, 2008: The equilibrium sensitivity of the earth's temperature to radiation changes. *Nat. Geosci.,* **1,** 735–743.

——, T. F. Stocker, F. Joos, and G. K. Plattner, 2002: Constraints on radiative forcing and future climate change from observations and climate model ensembles. *Nature,* **416,** 719–723.

——, G. A. Meehl, M. R. Allen, and D. A. Stainforth, 2006: Constraining climate sensitivity from the seasonal cycle in surface temperature. *J. Climate,* **19,** 4224–4233.

——, and Coauthors, 2008: A review of uncertainties in global temperature projections over the twenty-first century. *J. Climate,* **21,** 2651–2663.

——, R. Furrer, C. Tebaldi, J. Cermak, and G. A. Meehl, 2010: Challenges in combining projections from multiple climate models. *J. Climate,* **23,** 2739–2758.

Loeb, N. G., B. A. Wielicki, D. R. Doelling, G. L. Smith, D. F. Keyes, S. Kato, N. Manalo-Smith, and T. Wong, 2009: Toward optimal closure of the earth's top-of-atmosphere radiation budget. *J. Climate,* **22,** 748–766.

Meehl, G. A., and Coauthors, 2007: Global climate projections. *Climate Change 2007: The Physical Science Basis,* S. Solomon et al., Eds., Cambridge University Press, 747–845.

Murphy, J. M., D. M. H. Sexton, D. N. Barnett, G. S. Jones, M. J. Webb, and M. Collins, 2004: Quantification of modelling uncertainties in a large ensemble of climate change simulations. *Nature,* **430,** 768–772.

Ohmura, A., and H. Gilgen, 1991: Global Energy Balance Archive GEBA. Report 2: The GEBA data base, interactive applications, retrieving data. World Climate Programme Water Project A7, Zürcher Geographische Schriften Rep. 44, 66 pp.

——, and Coauthors, 1998: Baseline Surface Radiation Network (BSRN/WCRP): New precision radiometry for climate research. *Bull. Amer. Meteor. Soc.,* **79,** 2115–2136.

Onogi, K., and Coauthors, 2007: The JRA-25 Reanalysis. *J. Meteor. Soc. Japan,* **85,** 369–432.

Piani, C., D. J. Frame, D. A. Stainforth, and M. R. Allen, 2005: Constraints on climate change from a multi-thousand member ensemble of simulations. *Geophys. Res. Lett.,* **32,** L23825, doi:10.1029/2005GL024452.

Ramanathan, V., R. D. Cess, E. F. Harrison, P. Minnis, B. R. Barkstrom, E. Ahmad, and D. Hartmann, 1989: Cloud-radiative forcing and climate results from the Earth Radiation Budget Experiment. *Science,* **243,** 57–63.

Randall, D., and Coauthors, 2007: Climate models and their evaluation. *Climate Change 2007: The Physical Science Basis,* S. Solomon et al., Eds., Cambridge University Press, 589–662.

Sanderson, B. M., and Coauthors, 2008a: Constraints on model response to greenhouse gas forcing and the role of subgrid-scale processes. *J. Climate,* **21,** 2384–2400.

——, C. Piani, W. J. Ingram, D. A. Stone, and M. R. Allen, 2008b: Towards constraining climate sensitivity by linear analysis of feedback patterns in thousands of perturbed-physics GCM simulations. *Climate Dyn.,* **30,** 175–190.

——, K. Shell, and W. Ingram, 2009: Climate feedbacks determined using radiative kernels in a multi-thousand member ensemble of AOGCMs. *Climate Dyn.,* **35,** 1219–1236, doi:10.1007/s00382-009-0661-1.

Soden, B. J., and I. M. Held, 2006: An assessment of climate feedbacks in coupled ocean–atmosphere models. *J. Climate,* **19,** 3354–3360.

——, ——, R. Colman, K. M. Shell, J. T. Kiehl, and C. A. Shields, 2008: Quantifying climate feedbacks using radiative kernels. *J. Climate,* **21,** 3504–3520.

Stainforth, D. A., and Coauthors, 2005: Uncertainty in predictions of the climate response to rising levels of greenhouse gases. *Nature,* **433,** 403–406.

Stephens, G. L., 2005: Cloud feedbacks in the climate system: A critical review. *J. Climate,* **18,** 237–273.

Sutton, R. T., B. W. Dong, and J. M. Gregory, 2007: Land/sea warming ratio in response to climate change: IPCC AR4 model results and comparison with observations. *Geophys. Res. Lett.,* **34,** L02701, doi:10.1029/2006GL028164.

Tebaldi, C., and R. Knutti, 2007: The use of the multi-model ensemble in probabilistic climate projections. *Philos. Trans. Roy. Soc. London,* **A365,** 2053–2075.

Trenberth, K. E., and J. T. Fasullo, 2010: Simulation of present-day and twenty-first-century energy budgets of the southern oceans. *J. Climate,* **23,** 440–454.

——, ——, and J. Kiehl, 2009: Earth's global energy budget. *Bull. Amer. Meteor. Soc.,* **90,** 311–323.

Uppala, S. M., and Coauthors, 2005: The ERA-40 Re-Analysis. *Quart. J. Roy. Meteor. Soc.,* **131,** 2961–3012.

Vavrus, S., 2004: The impact of cloud feedbacks on Arctic climate under greenhouse forcing. *J. Climate,* **17,** 603–615.

Volodin, E. M., 2008: Relation between temperature sensitivity to doubled carbon dioxide and the distribution of clouds in current climate models. *Izv. Acad. Sci., USSR, Atmos. Oceanic Phys.,* **44,** 288–299.

Wielicki, B. A., B. R. Barkstrom, E. F. Harrison, R. B. Lee, G. L. Smith, and J. E. Cooper, 1996: Clouds and the Earth's Radiant Energy System (CERES): An Earth Observing System experiment. *Bull. Amer. Meteor. Soc.,* **77,** 853–868.

Wild, M., 2008: Short-wave and long-wave surface radiation budgets in GCMs: A review based on the IPCC-AR4/CMIP3 models. *Tellus,* **60A,** 932–945.

Zhang, Y., W. B. Rossow, A. A. Lacis, V. Oinas, and M. I. Mishchenko, 2004: Calculation of radiative fluxes from the surface to top of atmosphere based on ISCCP and other global data sets: Refinements of the radiative transfer model and the input data. *J. Geophys. Res.,* **109,** D19105, doi:10.1029/2003JD004457.